Nanoscale

Cite this: *Nanoscale*, 2012, **4**, 6870

www.rsc.org/nanoscale

PAPER

Tailored $Li_4Ti_5O_{12}$ nanofibers with outstanding kinetics for lithium rechargeable batteries†

Mi Ru Jo,[a] Yeon Sik Jung*[b] and Yong-Mook Kang*[a]

Received 30th June 2012, Accepted 10th September 2012
DOI: 10.1039/c2nr31675g

We report on the synthesis of one-dimensional (1D) $Li_4Ti_5O_{12}$ nanofibers through electrospinning and their outstanding electrochemical performances. $Li_4Ti_5O_{12}$ with a spinel structure is a promising candidate anode material for lithium rechargeable batteries due to its well-known zero-strain merits. In order to improve the electronic properties of spinel $Li_4Ti_5O_{12}$, which are intrinsically poor, we processed the material into a nanofiber type of architecture to shorten the Li^+ and electron transport distance using a versatile electrospinning approach. The electrospun $Li_4Ti_5O_{12}$ nanofiber showed significantly enhanced discharging/charging properties, even at high rates that exceeded 10 C, demonstrating that the nanofiber offers an attractive architecture for enhanced kinetics.

Introduction

The processing of materials with effective control at the nanometer scale regime has been actively pursued as a way of developing novel, innovative materials. In particular, the preparation of one-dimensional (1D) ceramic nanostructures such as fibers, wires, rods, belts, tubes, spirals, and rings have garnered great interest owing to the potential application of these structures in many technologically important areas, such as electronics, photonics, and mechanics, due to their low dimensionality, quantum confinement, and shape effects, which also makes them feasible for their use in optoelectronics, microelectronics and energy devices.[1–3] Energy-storage materials with 1D structure, such as nanofibers, nanowires and nanorods, typically have enhanced Li^+ reversibility and kinetic properties owing to the shortened distance for Li^+ transport and their innate structural robustness.[33,34] A lot of new synthetic methods for generating 1D nanostructures from various metal oxides have been demonstrated; notable examples include those based on the vapor–solid (VS),[4–6] vapor–liquid–solid (VLS),[7–9] solution–solid,[10] and solvothermal routes.[11,12] However, critical issues associated with these methods include insufficient yields and difficult manufacturability and size controllability.

Alternatively, electrospinning is regarded as one of the simplest and most versatile techniques. It is capable of generating 1D nanostructures easily and economically (mainly nanofibers; other types of 1D nanostructures, such as nanorods, can be cut from nanofibers by special methods[13,14]) from a variety of polymers.[15–20] Electrospinning is also an expandable technique, by which one can easily fabricate one-dimensional (1D) nanostructures with controllable diameters, compositions, and morphologies on an industrial scale.[21–27] In addition to the extensive controllability, its simplicity and cost-effectiveness, along with environmental-friendliness, make it a very promising methodology. The unique structural features such as the high surface area-to-volume ratio, extremely long length, and complex porous structure of the electrospun nanofibers make them suitable for various applications, especially for lithium rechargeable batteries.[28–30]

Among the candidates for next-generation anode materials, $Li_4Ti_5O_{12}$ using the Ti^{4+}/Ti^{3+} redox couple (*ca.* 1.55 V *vs.* Li/Li^+) has shown promising electrochemical properties, especially in terms of its feasible levels of structural and chemical stability. However, because the electronic structure of $Li_4Ti_5O_{12}$ characterized by empty Ti 3d states with a bandgap energy level of ~2 eV gives an insulating character to this material, the high rate performance of $Li_4Ti_5O_{12}$ may not be sufficient for high-power applications such as in energy storage systems (ESSs), hybrid electric vehicles (HEVs), or electric vehicles (EVs). In particular, for EV applications, developing energy-storage electrodes with excellent cyclability and capacity retention at high charge/discharge rates is a critical issue. Consequently, there have been several approaches which have focused on improving its rate capability by making conductive coating or/and reducing the particle size. As the representative examples, Park *et al.* reported that the TiN conductive layer on $Li_4Ti_5O_{12}$ enhances electrochemical properties at high current densities.[31] Lim *et al.* demonstrated that the nano-sized $Li_4Ti_5O_{12}$ anodes display a

[a]*Department of Chemistry, Dongguk University-Seoul, 100715 Seoul, Republic of Korea. E-mail: dake1234@dongguk.edu; Tel: +82-2-2260-8674*
[b]*Department of Materials Science & Engineering, Korea Advanced Institute of Science & Technology (KAIST), 291 Daehak-ro, Yuseong-gu, Daejeon 305-701, Republic of Korea. E-mail: ysjung@kaist.ac.kr*
† Electronic supplementary information (ESI) available. See DOI: 10.1039/c2nr31675g

clear electrochemical improvement especially at high current densities compared to micro-sized $Li_4Ti_5O_{12}$.[32]

This study reports the highly scalable synthesis method of $Li_4Ti_5O_{12}$ (LTO) nanofibers *via* electrospinning and the extensive controllability of their diameters by adjusting the e-spinning parameters. Collective analyses based on XRD and TEM confirm the good crystallinity of the calcined LTO nanofibers. Using this approach, the diameter of the nanofibers can easily be controlled in the nanometer regime, effectively increasing their specific surface area and improving the intercalation kinetics by providing a larger electrode–electrolyte contact area for Li^+ or electron transport. The electrospun LTO nanofibers exhibited greater capacity by nearly twofold compared to LTO nanopowders at high charge/discharge rates over 10 C, suggesting that this methodology is promising for high-power applications.

Experimental section

Preparation of $Li_4Ti_5O_{12}$ nanoparticles

$Li_4Ti_5O_{12}$ nanoparticles were prepared by a conventional solid-state reaction. Stoichiometric amounts of $LiOH \cdot H_2O$ and TiO_2 precursors were ball-milled in a container containing ethanol for 5 h and dried at 40 °C. The mixture was fired at 750 °C in air for 3 h. The color of the synthesized $Li_4Ti_5O_{12}$ nanoparticles was white. (See the image in the ESI, Fig. 4S.†)

Preparation of $Li_4Ti_5O_{12}$ nanofibers by electrospinning

Titanium(IV) isopropoxide ($Ti[OCH(CH_3)_2]_4$, 99%), lithium acetate dihydrate ($LiC_2H_3O_2 \cdot 2H_2O$, 99%), and poly(vinylpyrrolidone) (PVP, $M_w = 1\ 300\ 000$) were purchased from Aldrich. First, to prepare the electrospinning solution, 0.466 g of titanium(IV) isopropoxide and 0.134 g of lithium acetate (stoichiometric ratio of Li : Ti to 4 : 5) were mixed with 2 mL of ethanol and 1 mL of acetic acid. Following this, the solution was added to 2 mL of an ethanol solution containing 0.3 g of PVP. The solution then underwent stirring for 3 h. The mixture was immediately loaded into a plastic syringe equipped with a 27-gauge needle made of plastic. The needle was connected to a high-voltage supply that was generating a DC voltage of 15 kV. The feeding rate for the precursor solution was 0.5 mL h^{-1} using a syringe pump and the needle-to-collector distance was 13 cm. The electrospinning process was conducted in air. The electrospun products were calcined at 750 °C for three hours to remove any organics.

Structural characterization

$Li_4Ti_5O_{12}$ nanofibers were characterized by an XRD (Rigaku D/MAX-RB (12 kW) diffractometer using graphite-monochromatized Cu Kα radiation at 40 kV and 100 mA), a TEM (low resolution: Omega EM912 operated at 120 kV; high resolution: Philips F20Tecai operated at 200 kV), and a field emission scanning electron microscope (FE-SEM; TESCAN MIRA LMH2, operated at 15 kV). TGA (thermogravimetric analysis) has been done to figure out the compositional change of electrospun PVP/inorganic composite nanofibers during calcination.

Electrochemical measurements

Each electrode was fabricated by mixing each active material $Li_4Ti_5O_{12}$, acetylene black, and polyvinylidene fluoride (PVDF) at a weight ratio of 80 : 11 : 9 using *N*-methylpyrrolidone (NMP) as a solvent. The resulting slurries were pasted onto Al foils and then dried in a vacuum oven at 120 °C for 5 h. After drying, the electrode foils were pressed and then punched into a rectangle shape. The electrochemical properties of the prepared electrodes were evaluated using CR2016 coin-type cells assembled in an argon-filled glove box. Li metal foil was used as a counter electrode and 1 M solution of $LiPF_6$ in ethylene carbonate (EC) and dimethyl carbonate (DMC) (1 : 1, v/v) was employed as the electrolyte. The cells were charged and discharged galvanostatically between 1 V and 3.0 V at room temperature.

Results and discussion

$Li_4Ti_5O_{12}$ nanofibers were prepared by a modified electrospinning method. Fig. 1 shows a schematic illustration of the basic setup, consisting of a high-voltage power supply, a spinneret (a plastic needle), a collector (a piece of aluminum foil), and a syringe pump. The solution, composed of titanium isopropoxide, lithium acetate dihydrate and poly(vinylpyrrolidone) dissolved in ethanol, was loaded into a syringe with a spinneret at the tip. When this solution is ejected from the spinneret, the droplet becomes highly electrified immediately and the induced charges are evenly dispersed on the liquid surface. Under these conditions, two types of electrostatic force distort the droplet into a conical shape, forming the well-known Taylor cone. At the same time, the surface tension of the liquid and the electrostatic repulsion compete with each other. Once the latter overcomes the former, a jet is formed, which then undergoes a whipping motion due to a bending instability and quickly evolves into a solid fiber as a result of solvent evaporation.[15,35] As a result, PVP/inorganic composite nanofibers including lithium and titanium at the stoichiometric ratio of $Li_4Ti_5O_{12}$ were prepared for calcination. First, wide dimensional controllability of the electrospun nanofibers was demonstrated by changing the incorporated amount of PVP, which serves as a backbone in the electrospinning process.

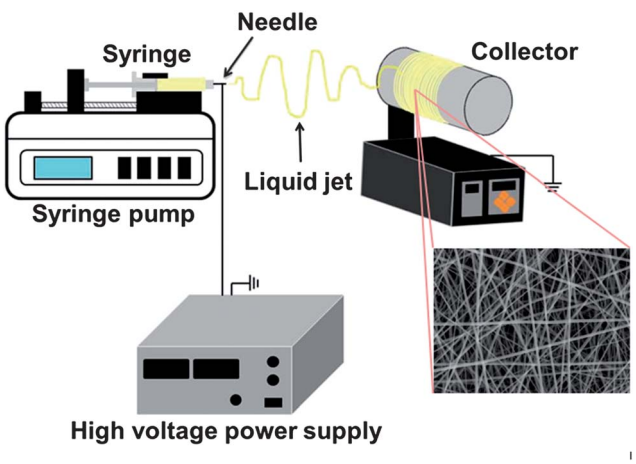

Fig. 1 The electrospinning setup for synthesizing electrospun $Li_4Ti_5O_{12}$ nanofibers.

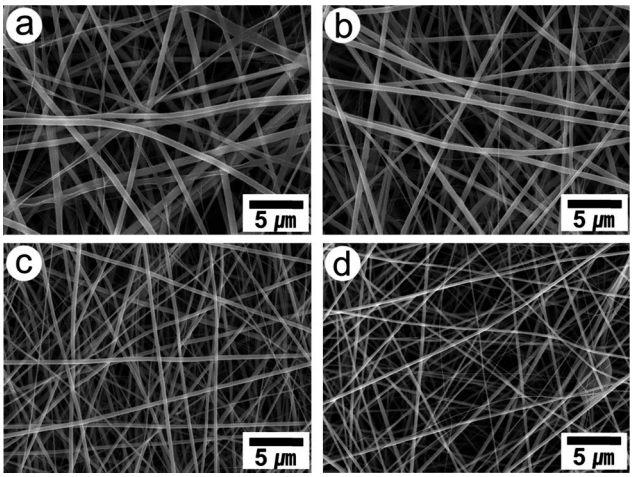

Fig. 2 SEM images of PVP/inorganic composite nanofibers that were electrospun from a mixture of PVP and inorganic precursors solved in ethanol. The weight ratio of PVP in the solution varied in the range of 5–8 wt %: (a) 8, (b) 7, (c) 6 and (d) 5.

Fig. 2 shows several representative SEM images of PVP/inorganic composite nanofibers which were electrospun from solutions with various concentrations of PVP. This figure clearly shows that the density of the beads and the diameter of the electrospun composite nanofiber are closely related to the concentration of PVP. When the concentration of the inorganic components (lithium and titanium precursors) was fixed for the starting materials (at a weight ratio of polymer to inorganic components of 1 : 2) and an electric field of 1.15 kV cm^{-1} was applied in our experiment, the average diameter of the PVP/inorganic composite fibers could be tuned in the ranges of 500 to 600 nm (Fig. 2a), 400 to 500 nm (Fig. 2b), 300 to 400 nm (Fig. 2c) and 200 to 300 nm (Fig. 2d) depending on the PVP concentration. Because the formation of beads should be prevented and the diameter of the electrospun nanofibers must be minimized to accelerate the electron transfer or Li ion transfer across them,[15] the electrospun nanofibers prepared with a PVP concentration of 6 wt% were chosen for use with the calcination process for $Li_4Ti_5O_{12}$ nanofibers.

To confirm the crystallinity of the calcined PVP/inorganic composite nanofibers, X-ray diffraction (XRD) and TEM analyses were conducted. The XRD patterns of the $Li_4Ti_5O_{12}$ nanoparticles prepared from a solid-state reaction and the electrospun $Li_4Ti_5O_{12}$ nanofibers after calcination are shown in Fig. 3a. According to the relevant literature, the diffraction peaks located at the 2θ of 18.331°, 30.181°, 35.571°, 37.212°, 43.242°, 47.352°, and 57.213° can be indexed to the crystal planes (111), (220), (311), (222), (400), (331), and (333) of spinel $Li_4Ti_5O_{12}$ (JCPDS #: 49-0207), respectively. All of the reflections were indexed in the *Fd*3*m* space group of the spinel structure. The results indicate that the $Li_4Ti_5O_{12}$ nanofibers were very well crystallized after calcination at 750 °C in ambient air. Although the PVP/inorganic composite nanofibers calcined at 700 and 800 °C also feature the characteristic spinel structure, as shown in Fig. S1,† the electrochemical results of all samples (Fig. S3†) suggest that 750 °C is the optimal calcination condition which enables the complete crystallization of electrospun PVP/

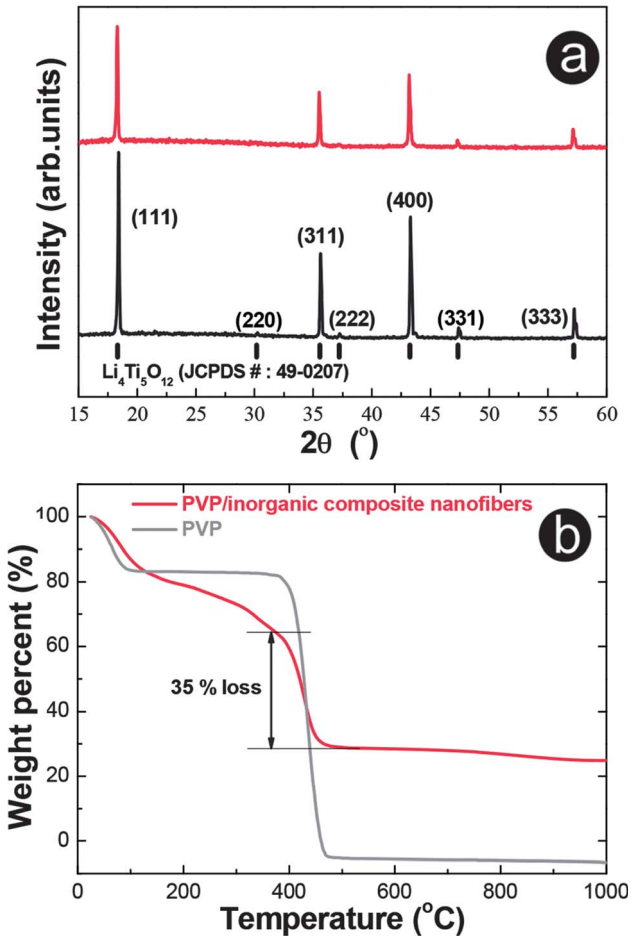

Fig. 3 (a) XRD patterns of $Li_4Ti_5O_{12}$ nanoparticles (black color) and polymer/inorganic composite nanofibers calcined at 750 °C (red color); (b) TGA results of PVP and PVP/inorganic composite nanofibers under N_2 atmosphere.

inorganic composite nanofibers while retaining their nanofiber morphologies. The TGA curve of PVP in Fig. 3b shows that PVP is completely decomposed and removed around 460 °C. The electrospun PVP/inorganic composite nanofiber undergoes 35% weight loss at the same temperature. The electrospun nanofiber is composed of 65–66% inorganic precursors and 34–35% PVP; this result clearly proves that the calcination at 750 °C is enough to completely remove the incorporated PVP. Hence, all contents in this work only originate from the intrinsic properties of $Li_4Ti_5O_{12}$ nanofibers.

The well-defined morphology of the calcined nanofibers was confirmed through SEM and TEM analyses. Fig. 4a shows the SEM image of an electrospun $Li_4Ti_5O_{12}$ nanofiber after calcination at 750 °C in ambient air. From this image, we found a characteristic fibrous morphology with uniform diameter less than 300 nm. SEM images of a $Li_4Ti_5O_{12}$ nanofiber obtained at other calcination temperatures are also shown in the ESI (Fig. S2†). All organic components could be removed from the electrospun fibers due to the high calcination temperature. TEM and HRTEM investigations were conducted for a further analysis of the secondary structures of the ultra-long hierarchical $Li_4Ti_5O_{12}$ nanofibers, as shown in Fig. 4b. Notably, the

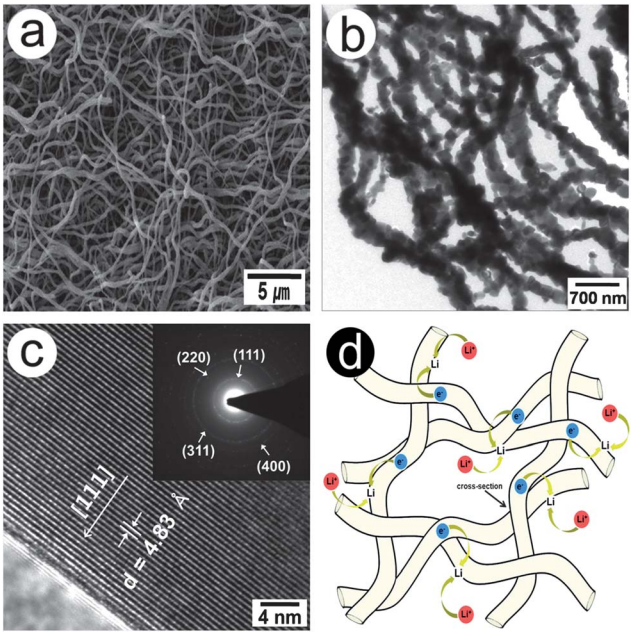

Fig. 4 (a) SEM image and (b) TEM image of electrospun $Li_4Ti_5O_{12}$ nanofibers after calcination in air at 750 °C, (c) high-resolution TEM image with indicated *d*-spacings and axes of the (111) planes (inset: selected-area electron diffraction pattern (SAED) of electrospun $Li_4Ti_5O_{12}$ nanofibers), and (d) a schematic diagram of the facilitated Li ion and electron transfer in electrospun $Li_4Ti_5O_{12}$ nanofibers.

nanorods were tightly attached to each other, thus constructing a typical nanofiber architecture. Clear and continuous lattice-fringe images of the electrospun $Li_4Ti_5O_{12}$ nanofiber are shown in Fig. 4c. The distance between neighboring fringes was measured to be 0.4835 nm, close to that of the (111) lattice spacing (0.483 nm) in a primitive cubic $Li_4Ti_5O_{12}$ lattice, which indicates that the structure of the formed nanofibers is attributed to the spinel $Li_4Ti_5O_{12}$.

A selected-area electron diffraction (SAED) image of the calcined electrospun $Li_4Ti_5O_{12}$ nanofibers is shown in Fig. 4d. The diffraction rings proving the polycrystalline nature of the final product can be indexed to the (111), (220), (331) and (440) planes of the spinel $Li_4Ti_5O_{12}$ phase. As suggested by numerous studies, the realization of the one-dimensional (1D) structure with large surface area and high length/diameter ratio is clearly accompanied by a significant kinetic enhancement.[29,31] Fig. 4d exemplifies that this may arise because the 1D structure can provide more reaction sites on the surface and its smaller diameter provides a shorter diffusion length for Li^+ insertion, therefore enhancing the charge transfer and electron conduction along the length direction.[36,37] The comparison between $Li_4Ti_5O_{12}$ nanofibers and nanoparticles in the BET surface area clearly indicates that the nanofiber structure can offer a larger reaction area toward Li^+ (Table S1†).

The electrospun $Li_4Ti_5O_{12}$ nanofibers exhibited superior electrochemical performance, including excellent cyclability over conventional nanoparticles. The electrochemical properties of the $Li_4Ti_5O_{12}$ nanoparticles and calcined electrospun $Li_4Ti_5O_{12}$ nanofibers were investigated by assembling Li/$Li_4Ti_5O_{12}$ half cells mixed with carbon black and polymer binder (see details in the Experimental section). Fig. 5a and b show their charge/discharge curves and cyclic performances, respectively, at a current density of 0.1 C. The electrospun $Li_4Ti_5O_{12}$ nanofibers show higher capacity and more stable capacity retention than the $Li_4Ti_5O_{12}$ nanoparticles up to 50 cycles. The charge/discharge characteristics of the nanofibers calcined at other temperatures are shown in the ESI (Fig. S3†). At low current densities below 1 C, the capacities of the electrospun $Li_4Ti_5O_{12}$ nanofibers do not differ much from those of the $Li_4Ti_5O_{12}$ nanoparticles. However, at high charge/discharge current densities that exceed 10 C, the capacities are nearly twofold compared to the $Li_4Ti_5O_{12}$ nanoparticles, proving the enhanced kinetics associated with their characteristic one-dimensional structure. In fact, there have been many reports showing that energy-storage materials with a one-dimensional structure, such as nanofibers, nanowires and nanorods, feature enhanced kinetic properties due to the shortened distance for ion transport and as a result of their innate structural robustness.[33,34]

Actually, the Nyquist plot from impedance analysis proves that electrospun $Li_4Ti_5O_{12}$ nanofibers feature drastically reduced film and charge transfer resistances compared to $Li_4Ti_5O_{12}$ nanoparticles in good accordance with the previous report on the enhanced kinetics of nanofiber structure (Fig. S5†). Furthermore, because the active materials are mixed with amorphous carbon for the electrode of lithium rechargeable batteries, the contact between the active materials and amorphous carbon is also a crucial factor determining the kinetics of the batteries (Fig. S6†). Hence, the fascinating electrochemical enhancement obtained from the electrospun $Li_4Ti_5O_{12}$ nanofibers can be attributed to not only the shortened distance for Li transport but also the increased contact area stemming from the fibrous 1D structure of these nanofibers (Fig. S6†).

From the results, it was evident that the electrospun $Li_4Ti_5O_{12}$ nanofibers have enhanced electrochemical performance compared to $Li_4Ti_5O_{12}$ nanoparticles, especially at a high charge/discharge rate. The specific capacities of the electrospun $Li_4Ti_5O_{12}$ nanofibers at 0.1 C and 10 C were 160 mA h g^{-1} and 138 mA h g^{-1} (86.25% retained), while the capacities of the $Li_4Ti_5O_{12}$ nanoparticles were 149 mA h g^{-1} and 71 mA h g^{-1} (47.7% retained), respectively (Fig. 5c). Fig. 5d depicts the galvanostatic intermittent titration curves, which show the slope at the beginning of the lithium insertion process and the subsequent voltage plateau around 1.5 V. The sloping curves indicate a single-phase region linked to a Li-incorporating solid solution reaction, and the voltage plateau part is characteristic of the two-phase equilibrium between the $Li_4Ti_5O_{12}$ and $Li_7Ti_5O_{12}$ during the Li^+ insertion process. This is known as the miscibility gap. The galvanostatic titration curves of electrospun $Li_4Ti_5O_{12}$ nanofibers show a typical miscibility gap extension compared to $Li_4Ti_5O_{12}$ nanoparticles, which leads to an increase in their discharge capacity.[38] The extended miscibility gap in electrospun nanofibers is believed to originate from the shortened distance for Li transport and the increased contact area with the conducting agent due to their fibrous 1D structure. Essentially, the initial polarization obtained from the difference between the closed-circuit voltage and open-circuit voltage (inset of Fig. 5d) is indicative of the enhanced kinetics of the electrospun 1D structure.

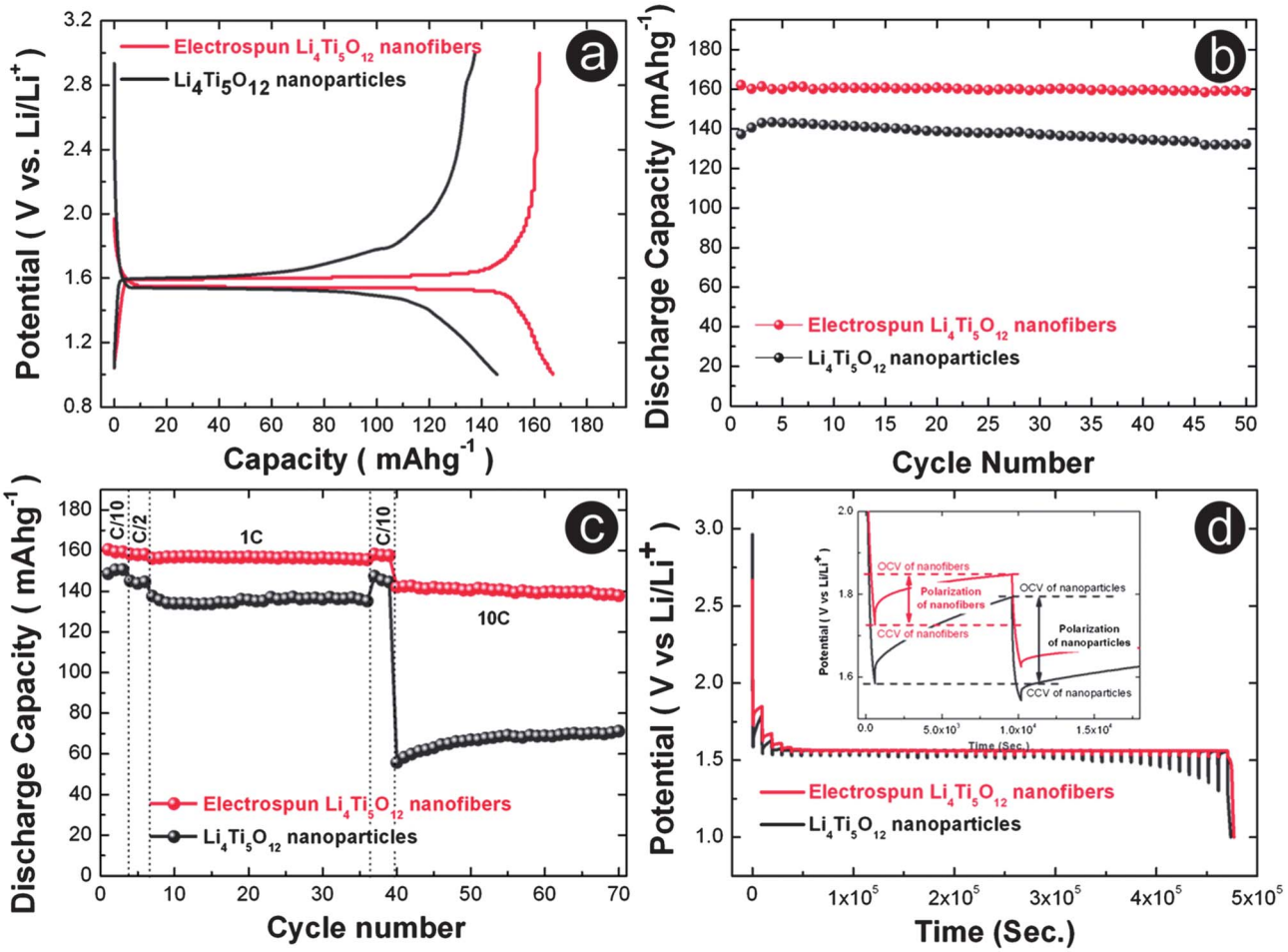

Fig. 5 The electrochemical performance of electrospun $Li_4Ti_5O_{12}$ nanofibers and $Li_4Ti_5O_{12}$ nanoparticles: (a) the initial galvanostatic charge/discharge curves at 0.1 C, (b) the cyclic performance at 0.1 C, (c) capacity retention amounts when conducting charge–discharge cycles at various current rates, (d) galvanostatic intermittent titration curves of electrospun $Li_4Ti_5O_{12}$ nanofibers and $Li_4Ti_5O_{12}$ nanoparticles.

Conclusions

In summary, $Li_4Ti_5O_{12}$ nanofibers with a typical 1D structure were successfully obtained *via* an electrospinning method. An electrochemical evaluation of the electrospun $Li_4Ti_5O_{12}$ nanofibers for lithium rechargeable batteries exhibits a high capacity with excellent cycle performance over 50 cycles. It was clearly proved that electrospinning can process the material into a nanosized 1D architecture to shorten the electron and Li^+ transport path and increase the surface-to-volume ratio. Furthermore, the high power density of $Li_4Ti_5O_{12}$ nanofibers was found to be excellent, implying the possibility of extended applications of lithium rechargeable batteries to high-power devices such as an energy storage system (ESS), hybrid electric vehicles (HEVs), electric vehicles (EVs), and portable power tools.

Acknowledgements

This research was supported by the Converging Research Center Program (2011K000974 and NRF-2010-C1AAA001-0029018) through the National Research Foundation of Korea funded by the Ministry of Education, Science, and Technology.

Notes and references

1 Y. Xia, P. Yang, Y. Sun, Y. Wu, B. Mayers, B. Gates, Y. Yin, F. Kim and H. Yan, *Adv. Mater.*, 2003, **15**, 353.
2 M. Law, J. Goldberger and P. Yang, *Annu. Rev. Mater. Res.*, 2004, **34**, 83.
3 Z. L. Wang, *Annu. Rev. Phys. Chem.*, 2004, **55**, 159.
4 Z. W. Pan, Z. R. Dai and Z. L. Wang, *Science*, 2001, **291**, 1947.
5 Y. Yin, G. Zhang and Y. Xia, *Adv. Funct. Mater.*, 2002, **12**, 293.
6 G. Gu, B. Zheng, W. Q. Han, S. Roth and J. Liu, *Nano Lett.*, 2002, **2**, 849.
7 R. S. Wagner and W. C. Ellis, *Appl. Phys. Lett.*, 1964, **4**, 89.
8 Y. Wu, H. Yan, M. Huang, B. Messer, J. H. Song and P. Yang, *Chem.–Eur. J.*, 2002, **8**, 1260.
9 C. H. Liang, G. W. Meng, G. Z. Wang, Y. W. Wang, L. D. Zhang and S. Y. Zhang, *Appl. Phys. Lett.*, 2001, **78**, 3202.
10 J. J. Urban, W. S. Yun, Q. Gu and H. Park, *J. Am. Chem. Soc.*, 2002, **124**, 1186.
11 Y. Li, H. Liao, Y. Ding, Y. Fan, Y. Zhang and Y. Qian, *Inorg. Chem.*, 1999, **38**, 1382.
12 X. Wang and Y. Li, *J. Am. Chem. Soc.*, 2002, **124**, 2880.
13 O. Kriha, M. Becker, M. Lehmann, D. Kriha, J. Krieglstein, M. Yesef, S. Schlecht, R. B. Wehrspohn, J. H. Wendorff and A. Greiner, *Adv. Mater.*, 2007, **19**, 2483.
14 A. Stoiljkovic and S. Agarwal, *Macromol. Mater. Eng.*, 2008, **293**, 895.
15 D. Li and Y. Xia, *Adv. Mater.*, 2004, **16**, 1151.
16 A. Greiner and J. H. Wendorff, *Angew. Chem., Int. Ed.*, 2007, **46**, 5670.

17 C. Burger, B. S. Hsiao and B. Chu, *Annu. Rev. Mater. Res.*, 2006, **36**, 333.
18 C. P. Barnes, S. A. Sell, E. D. Boland, D. G. Simpson and G. L. Bowlin, *Adv. Drug Delivery Rev.*, 2007, **59**, 1413.
19 D. Liang, B. S. Hsiao and B. Chu, *Adv. Drug Delivery Rev.*, 2007, **59**, 1392.
20 J. Xie, X. Li and Y. Xia, *Macromol. Rapid Commun.*, 2008, **29**, 1775.
21 D. Li and Y. Xia, *Nano Lett.*, 2003, **3**, 555.
22 I. G. Loscertales, A. Barrero, M. Marquez, R. Spretz, R. Velarde-Ortiz and G. Larsen, *J. Am. Chem. Soc.*, 2004, **126**, 5376.
23 Z. Liu, D. D. Sun, P. Guo and J. O. Leckie, *Nano Lett.*, 2007, **7**, 1081.
24 Y. Zhao, X. Cao and L. Jiang, *J. Am. Chem. Soc.*, 2007, **129**, 764.
25 J. Lin, B. Ding, J. Yu and Y. Hsieh, *ACS Appl. Mater. Interfaces*, 2010, **2**, 521.
26 E. Hosono, Y. Wang, N. Kida, M. Enomoto, N. Kohima, M. Okubo, H. Matsuda, Y. Saito, T. Kudo, I. Honma and H. Zhou, *ACS Appl. Mater. Interfaces*, 2010, **2**, 212.
27 Y. Yu, L. Gu, C. Zhu, P. A. V. Aken and J. Maier, *J. Am. Chem. Soc.*, 2009, **131**, 15984.
28 K. B. Tang, Y. T. Qian, J. H. Zeng and X. G. Yang, *Adv. Mater.*, 2003, **15**, 448.
29 M. H. Seo, M. Park, K. T. Lee, K. Kim, J. Kim and J. Cho, *Energy Environ. Sci.*, 2011, **4**, 425.
30 J. Hu, T. W. Odom and C. M. Lieber, *Acc. Chem. Res.*, 1999, **32**, 435.
31 K. S. Park, A. Benayad, D. J. Kang and S. G. Doo, *J. Am. Chem. Soc.*, 2008, **130**, 14930.
32 J. Lim, E. Choi, V. Mathew, D. Kim, D. Ahn, J. Gim, S. J. Kang and J. Kim, *J. Electrochem. Soc.*, 2011, **158**, A275.
33 C. K. Chan, H. Peng, G. Liu, K. Mcilwrath, X. F. Zhang, R. A. Huggins and Y. Cui, *Nat. Nanotechnol.*, 2008, **3**, 31.
34 L. Mai, Y. Dong, L. Xu and C. Han, *Nano Lett.*, 2010, **10**, 4273.
35 D. Li, J. T. McCann and Y. Xia, *J. Am. Ceram. Soc.*, 2006, **89**, 1861.
36 M. S. Park, G. X. Wang, Y. M. Kang, D. Wexler, S. X. Dou and H. K. Liu, *Angew. Chem., Int. Ed.*, 2007, **46**, 750.
37 K. Kang, H. S. Lee, D. W. Han, G. S. Kim, D. H. Lee, G. Lee, Y. M. Kang and M. H. Jo, *Appl. Phys. Lett.*, 2010, **96**, 053110.
38 M. R. Jo, K. M. Nam, Y. M. Lee, K. S. Song, J. T. Park and Y. M. Kang, *Chem. Commun.*, 2011, **47**, 11474.